

A *NuSTAR* and *Swift* View of the Hard State of MAXI J1813–095

Jiachen Jiang^{1,4*}, Douglas J.K. Buisson², Thomas Dauser³, Andrew C. Fabian¹, Felix Fürst⁵, Luigi C. Gallo⁶, Fiona A. Harrison⁷, Michael L. Parker¹, James F. Steiner⁸, John A. Tomsick⁹, Santiago Ubach⁸ and Dominic J. Walton^{10,1}

¹*Institute of Astronomy, University of Cambridge, Madingley Road, Cambridge CB3 0HA, UK*

²*Department of Astronomy, University of Southampton, Southampton SO17 1BJ, UK*

³*Dr Karl Remeis-Observatory and Erlangen Centre for Astroparticle Physics, Sternwartstr. 7, D-96049 Bamberg, Germany*

⁴*Department of Astronomy, Tsinghua University, 30 Shuangqing Road, Beijing 100084, China*

⁵*European Space Agency (ESA), European Space Astronomy Centre (ESAC), E-28691 Villanueva de la Cañada, Spain*

⁶*Department of Astronomy and Physics, Saint Mary's University, 923 Robie Street, Halifax, NS B3H 3C3, Canada*

⁷*Cahill Center for Astronomy and Astrophysics, California Institute of Technology, Pasadena, CA 91125, USA*

⁸*Harvard-Smithsonian Center for Astrophysics, 60 Garden Street, Cambridge, MA 02138, USA*

⁹*Space Sciences Laboratory, 7 Gauss Way, University of California, Berkeley, CA 94720-7450, USA*

¹⁰*Centre for Astrophysics Research, University of Hertfordshire, College Lane, Hatfield AL10 9AB, UK*

Accepted XXX. Received YYY; in original form ZZZ

ABSTRACT

We present an analysis of the *NuSTAR* and *Swift* spectra of the black hole candidate MAXI J1813–095 in a failed-transition outburst in 2018. The *NuSTAR* observations show evidence of reflected emission from the inner region of the accretion disc. By modelling the reflection component in the spectra, we find a disc inner radius of $R_{\text{in}} < 7 r_g$. This result suggests that either a slightly truncated disc or a non-truncated disc forms at a few per cent of the Eddington limit in MAXI J1813–095. Our best-fit reflection models indicate that the geometry of the innermost accretion remains consistent during the period of *NuSTAR* observations. The spectral variability of MAXI J1813–095 from multi-epoch observations is dominated by the variable photon index of the Comptonisation emission.

Key words: accretion, accretion discs - black hole physics, X-rays: binaries

1 INTRODUCTION

X-ray binaries are bright and variable X-ray emitters found in the Milky Way and nearby globular clusters (e.g. Hertz & Grindlay 1983; Jordán et al. 2004). Their X-rays are produced by the accretion process of materials from a donor star to a compact accretor, which is either a neutron star or a black hole (BH). Depending on the mass of the donor star, X-ray binaries are classified as low-mass and high-mass X-ray binaries. The donor star of a low-mass X-ray binary is usually less massive than the accretor, e.g. dwarf stars or main-sequence stars (e.g. Liu et al. 2007). In comparison, the donor of a high-mass X-ray binary is more massive, e.g. blue giants (e.g. Liu et al. 2006).

Some X-ray binaries show transient events featured by a boost of accretion rate along with a rapid increase of X-ray luminosity. The ‘soft’ state and the ‘hard’ state are the two most distinct spectral states in such outburst: the X-ray emission of an X-ray binary is dominated by the thermal emission of the accretion disc in the soft state and the non-thermal power-law emission from the corona in the hard state (e.g. Oda et al. 1971; Cui et al. 1998; Rao et al. 2000;

Yu & Yan 2009; Shidatsu et al. 2011; Reis et al. 2013). Such a change of state often shows the so-called ‘q’-shaped pattern in the X-ray hardness-intensity diagram (e.g. Fender et al. 2004; Homan et al. 2005; Dunn et al. 2010). Other intermediate states have also been identified during the transition phases between the canonical ‘soft’ and ‘hard’ states (e.g. Done et al. 2007). A few sources among known X-ray binaries never reached the soft state during an outburst (e.g. Brocksopp et al. 2004; Sturmer & Shrader 2005; Jiang et al. 2020a), which is often referred to as a failed-transition outburst.

In the ‘no-hair theorem’, an astrophysical BH is described by just its mass and spin (for a review, see Chruściel et al. 2012, the third parameter electrical charge being effectively neutral in an astrophysical setting). Understanding BH spin is important in different aspects. For example, the spins of the BHs have been proposed to be the energy source behind energetic jets launched from BHs. This assumption was supported by both theories and observations (e.g. Blandford & Znajek 1977; Tchekhovskoy et al. 2011; McClintock et al. 2014). Two techniques have been commonly used to measure BH spins, the X-ray continuum-fitting method (Zhang et al. 1997) and the relativistic disc reflection spectroscopy (Fabian et al. 1989). They both rely on the monotonic relationship between BH spin and the radius of the innermost stable circular orbit

* E-mail: jj447@cam.ac.uk

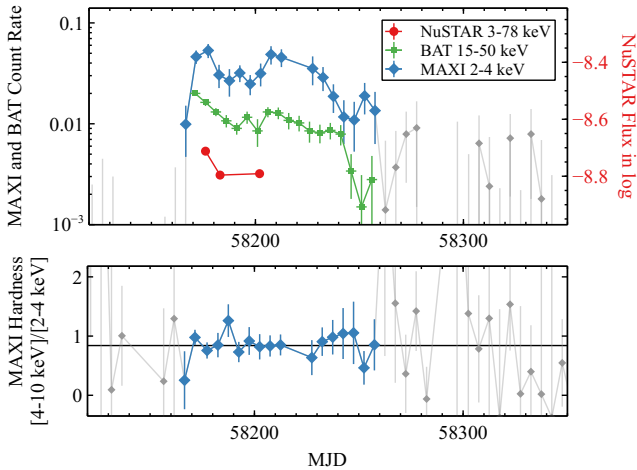


Figure 1. Top: *MAXI* (blue and grey diamonds), *Swift*-BAT (green squares) and *NuSTAR* lightcurves (red circles) of MAXI J1813 in outburst in 2018. The error bars of the *NuSTAR* lightcurves are smaller than the size of the circles. Bottom: *MAXI* hardness ratio curve of MAXI J1813.

(ISCO) for orbiting particles around a BH. It is, therefore, essential to study whether the disc extends to the ISCO or is truncated during a certain observation, which determines the validity of the two methods for BH spin measurements.

Esin et al. (1997) suggested that the inner accretion disc of a BH X-ray binary might be indeed truncated in a low luminosity state. Instead, an advection-dominated accretion flow onto the BH appears in the low-flux/hard state (e.g. Quataert & Narayan 1999). But the degree to which the discs of BH X-ray binaries are truncated in the hard state at a modest luminosity, e.g. 1%-10% of L_{Edd} , is still a controversial question. Recent work on this topic focused on the modelling of the disc reflection spectra in the X-ray band: some found discs are either close to ISCO or slightly truncated (e.g. in GX 339–4, García et al. 2015; Fürst et al. 2015); while others found that the discs are significantly truncated (e.g. $300 r_g$ for GX 339–4, Plant et al. 2015). Intermediate values of R_{in} , e.g. a few tens of r_g , were also obtained (e.g. Cyg X–1, Basak et al. 2017). It is important to note that, if the thin disc is truncated at $100\text{--}300 r_g$, the coronal region, which illuminates the disc, has to extend to a similar size to produce the observed amount of reflection. Such a large size would bring challenges in explaining the steep disc emissivity profiles (Fabian et al. 2012) and the observed reverberation lags in the hard state (De Marco et al. 2013; Kara et al. 2019). The diametrically opposed conclusions might be due to calibration issues in timing-mode data from CCDs, e.g. on *XMM-Newton* and the usage of different models (Kolehmainen et al. 2013; García et al. 2015).

In this work, we study the geometry of the innermost accretion region of MAXI J1813–095 in the hard state by modelling its broad band X-ray spectra. MAXI J1813–095 (MAXI J1813 hereafter) is an X-ray binary discovered by *MAXI* that had a failed-transition X-ray outburst in 2018 (Kawase et al. 2018). The nature of the compact object in MAXI J1813 has not been dynamically confirmed. However, the X-ray band of MAXI J1813 is dominated by non-thermal power-law emission as in the hard state of typical BH transients (Fuerst et al. 2018; Armas Padilla et al. 2019).

Figure 1 shows the X-ray lightcurves of MAXI J1813 in 2018. MAXI J1813 quickly reached the peak X-ray flux within the first 10 days. Then the outburst lasted for around 90 days before returning to the quiescent state. The lower panel of Figure 1 shows the

MAXI hardness ratio curve for the same period (Matsuoka et al. 2009), which remains consistent during the whole outburst¹. Detailed spectral analysis of *INTEGRAL*, *NICER* and *XMM-Newton* data suggests that MAXI J1813 remains in the hard state during the outburst (Fuerst et al. 2018; Armas Padilla et al. 2019; Jana et al. 2021).

In this work, we analyse three sets of *NuSTAR* and *Swift* observations of MAXI J1813 in outburst. We focus on the modelling of their X-ray spectra. In particular, we try to probe the geometry of the innermost accretion region of MAXI J1813 in the hard state, e.g. whether the disc is truncated at a large radius (e.g. Plant et al. 2015) or close to the BH (e.g. García et al. 2015).

In Section 2, we introduce our data reduction processes. In Section 3, we present a detailed analysis of the stacked *NuSTAR* and *Swift* spectra of MAXI J1813 considering various reflection models. In Section 4, we study the multi-epoch variability of MAXI J1813 based on the best-fit reflection model. In Section 6, we conclude our results.

2 DATA REDUCTION

2.1 *NuSTAR*

We reduced the *NuSTAR* data using the *NuSTAR* Data Analysis Software (NuSTARDAS) package and calibration data of V20200510. The energy spectra of MAXI J1813 were extracted for both the FPMA and FPMB detectors from a $100''$ radius circle centered on the source, while the background spectra were extracted from source-free polygon regions on the same detector chip. We consider the 3–78 keV band of the two FPM spectra.

2.2 *Swift*

The X-ray Telescope (XRT) data from the *Swift* observation were reduced using XRTPIPELINE version 0.13.4. The calibration file version is V20200726. The observation was operated in the Window Timing mode. Source spectra were extracted from a radius of 20 pixels². The background region was chosen to be an annular region with an inner radius of 50 pixels and an outer radius of 70 pixels. The 0.5–10 keV band of the XRT data is considered in this work.

All the spectra are grouped to have a minimum signal-to-noise of 6 per bin and oversample by a factor of 3. We use XSPEC V12.11.1 (Arnaud 1996) for spectral analysis, and χ^2 is used for the goodness-fit test in this work. The uncertainties are given at the 90% confidence level unless specifically mentioned otherwise.

3 STACKED SPECTRAL ANALYSIS

The hardness ratio of MAXI J1813 remained at a similar level in the period of three *NuSTAR* observations: the flux ratio between 3–10 keV and 1–3 keV bands is around 2.6–2.7 measured by *NuSTAR* (see Table 1). A quick view of the spectra is given in Fig. 2. The spectra of the three epochs share a similar spectral shape. We therefore start our analysis with the averaged spectra of MAXI J1813 averaged from all three epochs. The ADDSPEC tool is used to stack spectra.

¹ Interested readers can find the *Swift* hardness-intensity diagram of this outburst in Jana et al. (2021).

² Each pixel is approximately $2.36''$.

Table 1. A list of observations of MAXI J1813 taken in 2018. The last three columns show the observed flux of MAXI J1813 in the 1–3, 3–10 and 10–78 keV bands in units of 10^{-10} erg cm^{-2} s^{-1} . The 3–10 and 10–78 keV flux of MAXI J1813 are the mean values of FPMA and FPMB measurements. The 3–10 keV flux measured by XRT is shown in the brackets. The 1–3 keV flux is measured by XRT.

<i>NuSTAR</i>	Date	Exposure	<i>Swift</i>	Date	Exposure	$F_{1-3\text{keV}}$ XRT (10^{-10} erg cm^{-2} s^{-1})	$F_{3-10\text{keV}}$ FPM (XRT) (10^{-10} erg cm^{-2} s^{-1})	$F_{10-78\text{keV}}$ FPM (10^{-10} erg cm^{-2} s^{-1})
		(ks)			(ks)			
80402303002	02-28	20.5	00088654001	02-27	1.9	1.55 ± 0.02	4.21 ± 0.02 (4.31 ± 0.05)	15.20 ± 0.02
80402303004	03-06	20.4	00088654002	03-06	1.8	1.28 ± 0.02	3.50 ± 0.02 (3.56 ± 0.04)	12.51 ± 0.02
80402303006	03-25	23.2	00088654004	03-25	2.0	1.49 ± 0.02	3.84 ± 0.02 (3.87 ± 0.05)	12.32 ± 0.02

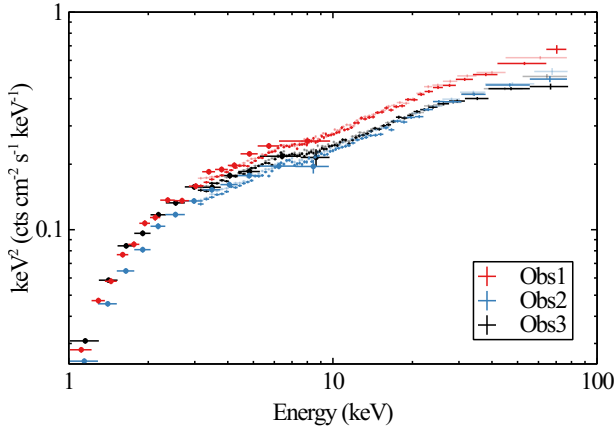


Figure 2. X-ray spectra of MAXI J1813 (Red: Obs1; blue: Obs2; black: Obs3). The spectra are corrected for the effective area of the instruments but not unfolded from the instrumental response. Data from XRT, FPMA and FPMB are plotted, but shown in the same colour to ease comparison between epochs. Crosses: FPMA; fainter crosses: FPMB; circles: XRT.

To start with, we fit the spectra with an absorbed Comptonisation model. The `nthcomp` model is used to calculate the Comptonisation spectrum (Życki et al. 1999), and the `tbnew` model is used to account for Galactic absorption (Wilms et al. 2006). The data/model ratio plot is shown in Figure 3. Evidence of a broad emission line around 6.4 keV and a hump feature above 10 keV is found in the *NuSTAR* spectra, suggesting the existence of a reflection component in the data. An additional distant, ionised reflector `xillvercp` (García & Kallman 2010) fails to fit the broad emission line with significant residuals in the iron emission band (see the third panel). This suggests that the reflection component originates in the inner region of the accretion disc where relativistic corrections are required (e.g. Fabian et al. 1989).

In this section, we introduce three models for the disc reflection component in the spectra of MAXI J1813, one with a power-law disc emissivity profile, one for a disc illuminated by an isotropic point-like corona, i.e. in the ‘lamppost’ geometry and a high-density disc reflection model.

3.1 `relxillcp`

We first apply the `relxillcp` model to the spectra of MAXI J1813 (Dauser et al. 2013; García & Kallman 2010). This model calculates relativistic disc reflection spectra by given seed photon spectra in the shape of `nthcomp`. We allow the reflection fraction (f_{refl}) in the model to be a positive, free parameter in our spectral fitting. So, the model includes both the disc reflection component and the

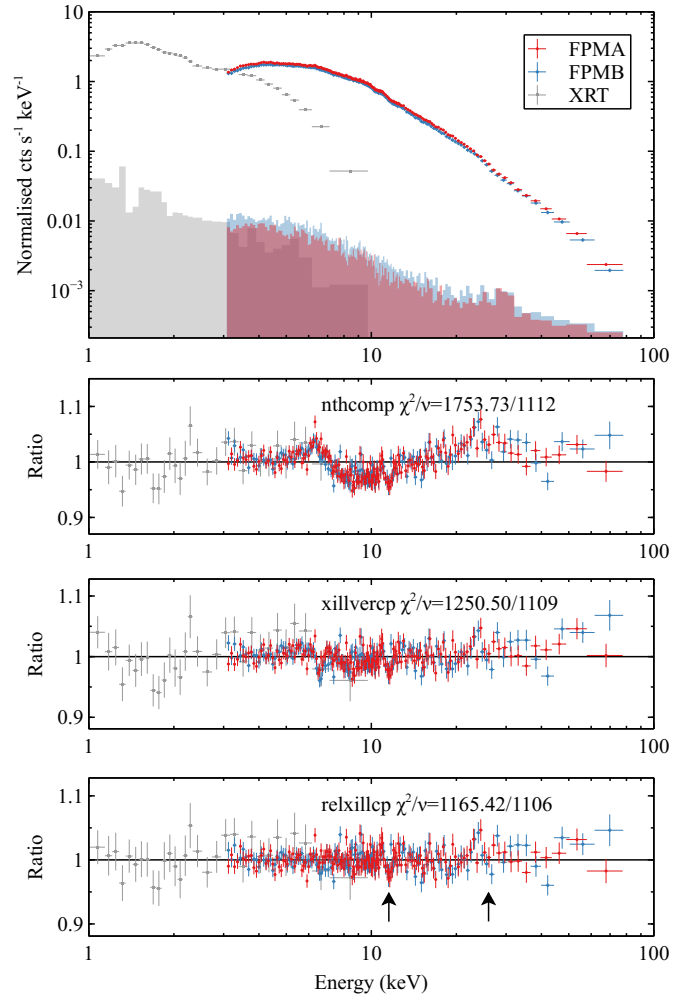


Figure 3. Top: *NuSTAR* (red: FPMA; blue: FPMB) and *Swift* (grey: XRT) source (crosses) and background spectra (shaded regions) of MAXI J1813. Bottom three panels: data/model ratio plots using different models. FPM spectra show evidence of broad emission line around 6.4 keV and a hump feature above 10 keV, suggesting existence of a reflection component. A distant, ionised reflector (`xillvercp`) fails to fit the spectra with significant residuals around the iron emission band as shown in the third panel. A relativistic disc reflection model (`relxillcp`) is therefore used to improve the fit. The residuals at 12 and 28 keV marked by the black arrows are due to instrumental features (Madsen et al. 2015).

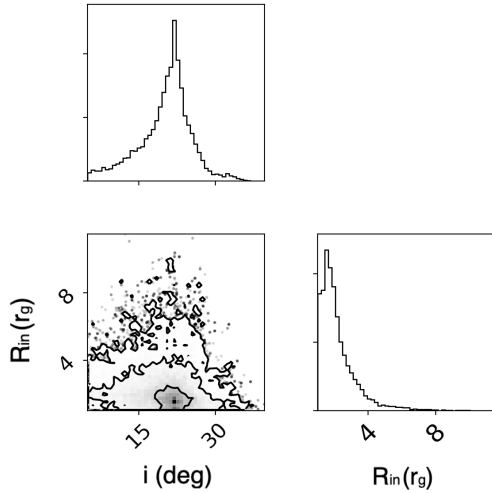


Figure 4. Output distributions of MCMC analysis based on the `relxillcp` model. Contours correspond to 1, 2 and 3 σ uncertainty ranges.

Table 2. Best-fit parameters for the averaged *NuSTAR* and *Swift* spectra of MAXI J1813. Note that the values of f_{refl} of `relxillcp` and `relxillpcp` are not comparable as different geometries of the corona are assumed. The quoted errors are at the 90% confidence level.

Parameters	<code>relxillcp</code>	<code>relxillpcp</code>	<code>reflionx</code>
N_{H} (10^{21} cm^{-2})	8.09 ± 0.02	$8.091^{+0.019}_{-0.016}$	9.50 ± 0.04
q	$2.5^{+0.7}_{-0.3}$	-	-
h (r_{g})	-	11^{+6}_{-4}	14^{+7}_{-5}
i (deg)	22^{+8}_{-9}	23^{+6}_{-11}	20^{+7}_{-10}
R_{in} (r_{g})	<5	<7	<7
Γ	1.644 ± 0.006	1.644 ± 0.007	$1.682^{+0.005}_{-0.007}$
kT_{e} (keV)	>180	>190	>170
Z_{Fe} (Z_{\odot})	$1.6^{+0.4}_{-0.6}$	$1.7^{+0.4}_{-0.5}$	1.1 ± 0.3
n_{e} (cm^{-3})	10^{15}	10^{15}	10^{19}
f_{refl}	0.08 ± 0.02	$0.19^{+0.02}_{-0.04}$	-
$\log(\xi/\text{erg cm s}^{-1})$	$3.10^{+0.09}_{-0.06}$	$3.10^{+0.07}_{-0.06}$	$2.13^{+0.12}_{-0.09}$
Norm (10^{-3})	4.31 ± 0.03	$5.8^{+0.3}_{-0.4}$	$2.4^{+2.3}_{-0.4} \times 10^3$
Norm _{pl}	-	-	0.11 ± 0.03
C_{FPMB}	1.025 ± 0.003	1.025 ± 0.003	1.024 ± 0.003
C_{XRT}	1.03 ± 0.02	1.03 ± 0.03	1.03 ± 0.03
χ^2/ν	1165.42/1106	1166.35/1106	1164.27/1106

coronal Comptonisation component. Other free parameters include the inner disc radius³ (R_{in}), the inclination angle of the disc (i), the emissivity index (q), the iron abundance of the disc (Z_{Fe}) and the ionisation of the disc (ξ). A constant density of $n_{\text{e}} = 10^{15} \text{ cm}^{-3}$ is assumed for the disc in this model. A constant model is used to account for cross-calibration uncertainties between instruments. The full model is `constant * tbnew * relxillcp` in XSPEC notation.

In this `relxillcp` model, we calculate the reflection spectrum of the disc taking all the relativistic effects into account, and the fit is significantly improved with $\Delta\chi^2 = 85$ and three more free

parameters compared to the fit using the distant reflection model `xillvercp`. Best-fit parameters are given in the first column of Table 2, and corresponding data/model ratio plots are shown in the bottom panel of Figure 3. The values of the constant models are within the expectations based on the cross-calibration work in (Madsen et al. 2015).

We add an additional `diskbb` component to account for any possible disc thermal emission. The fit is not significantly improved $\Delta\chi^2 < 2$ and two more free parameters. We, therefore, conclude that no significant thermal emission from the disc is found in our data (see Appendix A for more discussion). We note that a disc thermal component was identified by Jana et al. (2021) using the same *NuSTAR* and *Swift* observations. The requirement for an additional disc thermal component is based on a simple phenomenological model where Fe K emission is fit by a relativistic disc line model. The contribution of disc reflection in the soft and hard X-ray band is ignored.

The best-fit `relxillcp` model suggests a thin disc with an inner radius of $R_{\text{in}} < 5 r_{\text{g}}$ forms around the BH during our observations. The small value of R_{in} indicates either a slightly truncated disc or a disc that extends to the innermost stable circular orbit exists in the hard state of MAXI J1813. Besides, the model implies an almost face-on viewing angle of 22° for the disc.

We further estimate measurement uncertainties using the MCMC algorithm. The XSPEC/EMCEE code based on (Foreman-Mackey et al. 2013) of the Goodman-Weare affine invariant MCMC ensemble sampler (Goodman & Weare 2010) is used for this purpose. We use 200 walkers with a length of 100000, burning the first 10000. A convergence test has been conducted and the Gelman-Rubin scale-reduction factor $R < 1.3$ for every parameter. No obvious degeneracy is found. The contour plots of R_{in} and i are shown in Figure 4. The uncertainties given by MCMC analysis are consistent with the values obtained by the `ERROR` command in XSPEC. For instance, the 3- σ upper limit of R_{in} is $8 r_{\text{g}}$ when using the `relxillcp` model.

3.2 `relxillpcp`

So far, we have obtained a good fit using the `relxillcp` model. A power-law emissivity profile of ($F \propto r^{-q}$) is used in this model, and no particular geometry is assumed for the coronal region⁴.

In this section, we consider the lamppost geometry for the innermost region of the disc (Martocchia & Matt 1996). In particular, we investigate whether the choice of the lamppost geometry affects our measurements of the geometry of the innermost accretion region in MAXI J1813. The `relxillpcp` model is used (Dauser et al. 2016) for this purpose. Instead of a power-law emissivity profile, `relxillpcp` calculates emissivity profiles depending on h , the height of the corona above the BH on its rotational axis.

By applying the `relxillpcp` model to the spectra, we also find a good fit with $\chi^2/\nu = 1166.35/1106$. The goodness of the fit is consistent with that of `relxillcp`. The best-fit model and corresponding data/ratio plots are shown in Figure 5. MCMC analysis is also used to estimate measurement uncertainties.

When the `relxillpcp` model is used, the upper limit of R_{in} increases slightly: the 2- σ upper limit of R_{in} is $6 r_{\text{g}}$ (see Fig. 6). In

³ The BH spin parameter is fixed at 0.998.

⁴ Disc emissivity profiles were calculated for various coronal geometries, e.g. sphere and jet-like (Gonzalez et al. 2017). A power law or a broken power law is found to be a good approximation for their emissivity profiles (Wilkins & Fabian 2012; Gonzalez et al. 2017).

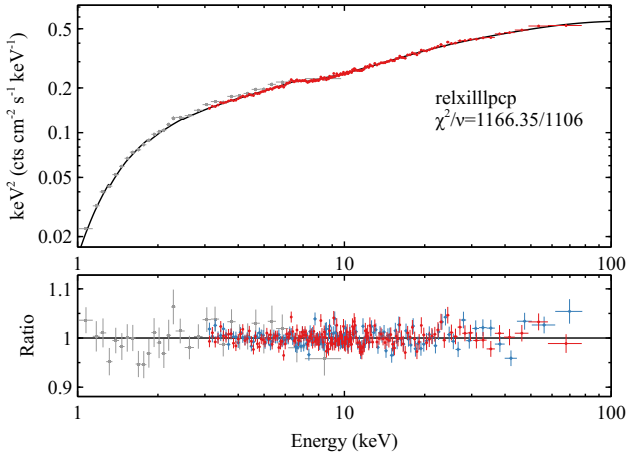


Figure 5. Top: the best-fit `relxill1pcp` model (black line) and unfolded FPMA (red) and XRT (grey) spectra of MAXI J1813. Bottom: corresponding data/model ratio plots.

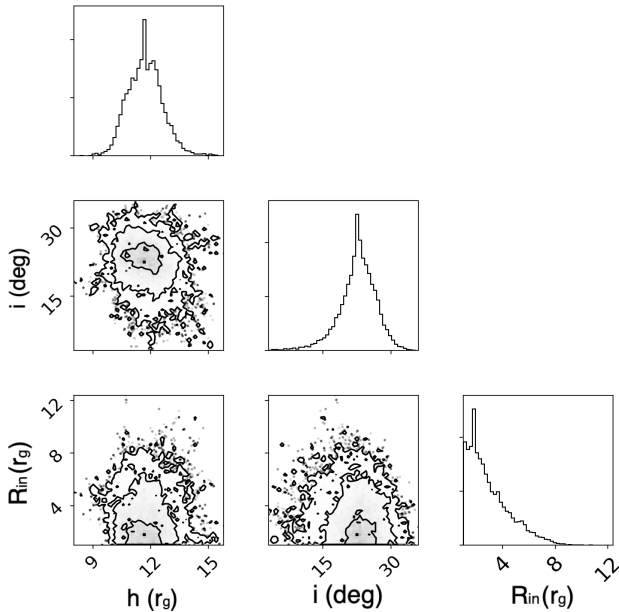


Figure 6. Same as Figure 4 but based on the `relxill1pcp` model.

comparison, the $2\text{-}\sigma$ upper limit given by the `relxill1pcp` model is $4 r_g$. However, their measurements of R_{in} are similar. The inferred inclination angles from two models are also consistent. Our `lamppost` model also suggests a coronal region that extends to $h = 11^{+3}_{-4} r_g$.

3.3 reflionx

Recently, it has been found that a high disc electron density of over $n_e = 10^{19} \text{ cm}^{-3}$ is required to explain the reflection spectra of BH transients in various states (Tomsick et al. 2018; Jiang et al. 2019a, 2020a; Connors et al. 2021). This model provides a possible solution

to inferred supersolar iron abundances in previous reflection models (Tomsick et al. 2018; Jiang et al. 2018, 2019b).

We test a high density disc reflection model with the `reflionx` model (Ross & Fabian 2007). The `reflionx` is calculated with `nthcomp`-shaped illuminating spectra (Jiang et al. 2020b). The `relconvlp` model is applied to the `reflionx` model to account for relativistic corrections. The full model is `constant * tbnew * (relconvlp * reflionx + nthcomp)` in XSPEC notation. In comparison with the `relxill1pcp`, this model has one additional parameter, the electron density of the disc surface (n_e).

By applying the `reflionx` model to the data, we only find an upper limit for the n_e parameter of 10^{21} cm^{-3} . The χ^2 distribution against n_e is shown in Figure 8. Tentative evidence of $n_e = 10^{19} \text{ cm}^{-3}$ is suggested by our fit. But $\Delta\chi^2$ is lower than 1.2 in the range of $10^{15} - 10^{20} \text{ cm}^{-3}$. The poorly constrained density parameter is likely due to the lack of evidence of blackbody-like emission in the *Swift* data of MAXI J1813. As shown in Figure 3, the XRT spectrum is consistent with an absorbed power law below 3 keV. At a high density, the disc reflection spectrum shows a blackbody-like emission due to stronger free-free absorption.

We show the upper limit of n_e of MAXI J1813 in comparison with other BH transients in the right panel of Figure 8. GX 339–4 and GRS 1716–249 show a variable density parameter during their outburst (Jiang et al. 2019a, 2020a). A lower limit of $n_e = 10^{20} \text{ cm}^{-3}$ is found in all spectral states of 4U 1630–47 (Connors et al. 2021).

We further investigate whether a high density model would affect our measurements of R_{in} and i . We fix $n_e = 10^{19} \text{ cm}^{-3}$, where the minimum χ^2 is found. Then we fit the spectra with all the other parameters free to vary. We obtain a similar upper limit for $R_{\text{in}} (< 7 r_g)$ and a similar disc inclination angle ($i \approx 20^\circ$). The best-fit parameters are shown in the last column of Table 2, and the best-fit model is shown in Figure 7. Most of the parameters are consistent with the values obtained by the `relconvlp` model except for the ionisation parameter of the disc and the line-of-sight column density. The ionisation parameter ($\log(\xi)$) of this high-density model is lower than the inferred values of best-fit low-density models. A slightly higher column density of $N_{\text{H}} = 9.50 \pm 0.04 \times 10^{21} \text{ cm}^{-2}$ is found⁵. This is due to the blackbody-like emission in the high density disc model, where free-free absorption increases the temperature of the disc surface (Ross & Fabian 2007; Garca et al. 2016). A slightly higher N_{H} is therefore required when $n_e = 10^{19} \text{ cm}^{-3}$ is used in the model.

4 INDIVIDUAL OBSERVATIONS

So far, we have modelled the stacked spectra of MAXI J1813 in the hard state. By applying a `lamppost` model to the data, we obtain $R_{\text{in}} < 7 r_g$ and $i = 12^\circ - 29^\circ$. Consistent measurements are achieved when a power-law emissivity profile or a high density disc model is considered, suggesting the measurements are independent from the coronal geometry and the density parameter.

In this section, we apply the `relxill1pcp` to each individual epoch to study their spectral variability. Only an upper limit of n_e is found for the stacked spectra. Therefore, we do not consider a variable density parameter in the following analysis. The inclination

⁵ The line-of-sight Galactic column density of H I and H₂ combined is estimated to be $5.4 \times 10^{21} \text{ cm}^{-2}$ (Willingale et al. 2013), which is lower than the inferred values from our observations. Similar results were found in *XMM-Newton* and *INTEGRAL* spectral analysis (Fuerst et al. 2018; Armas Padilla et al. 2019).

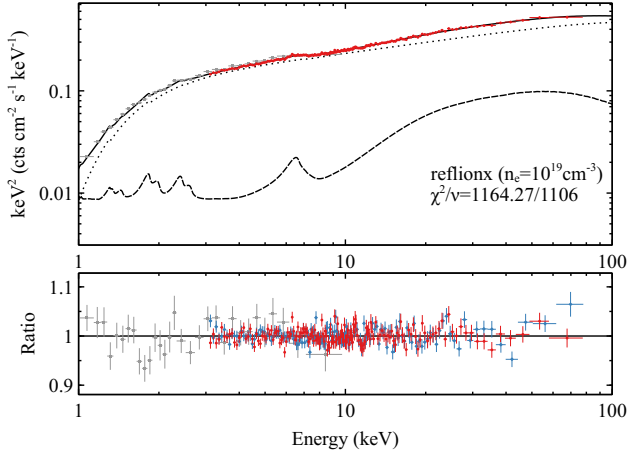


Figure 7. Top: the best-fit model with $n_e = 10^{19} \text{ cm}^{-3}$ (solid black line) and unfolded FPMA (red) and XRT (grey) spectra of MAXI J1813. Dotted line: the Comptonisation component; dash-dotted line: the disc reflection component. Bottom: corresponding data/model ratio plots.

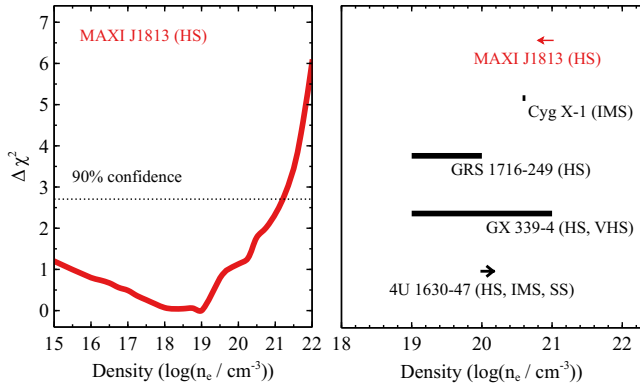


Figure 8. Left: $\Delta\chi^2$ vs. n_e obtained by fitting the spectra of MAXI J1813 with `reflionx`. Only an upper limit of $n_e (< 10^{21} \text{ cm}^{-3})$ is found for the disc in MAXI J1813. Right: n_e of MAXI J1813 in comparison with the measurements of other BH transients (Tomsick et al. 2018; Jiang et al. 2019a, 2020a; Connors et al. 2021). HS: the hard state; IMS: the intermediate state; VHS: the very high state; SS: the soft state.

angle and the iron abundances are not expected to be variable on observable timescales. Therefore, they are linked between epochs. The best-fit parameters of the `relxill1pcp` models for three epochs are shown in Table 3. Best-fit models are shown in Figure 9. The `relxill1pcp` model provides a good fit to all three sets of spectra.

Based on our best-fit models, we find that the unabsorbed X-ray flux of MAXI J1813 varies between $2.3 - 2.8 \times 10^{-9} \text{ erg cm}^{-2} \text{ s}^{-1}$ in the 0.01–100 keV band. Assuming a distance of 8 kpc⁶ (Russell et al. 2018), they correspond to $1.8 - 2.1 \times 10^{37} \text{ erg s}^{-1}$. The mass of the BH in MAXI J1813 is unknown. Assuming a typical BH

⁶ Based on the stellar populations of the Galactic disc and bulge (Juric et al. 2008), a source along the line of sight of MAXI J1813 has a likely distance of 8_{-2}^{+6} kpc (1σ) excluding the effect of any natal supernova kicks (Russell et al. 2018).

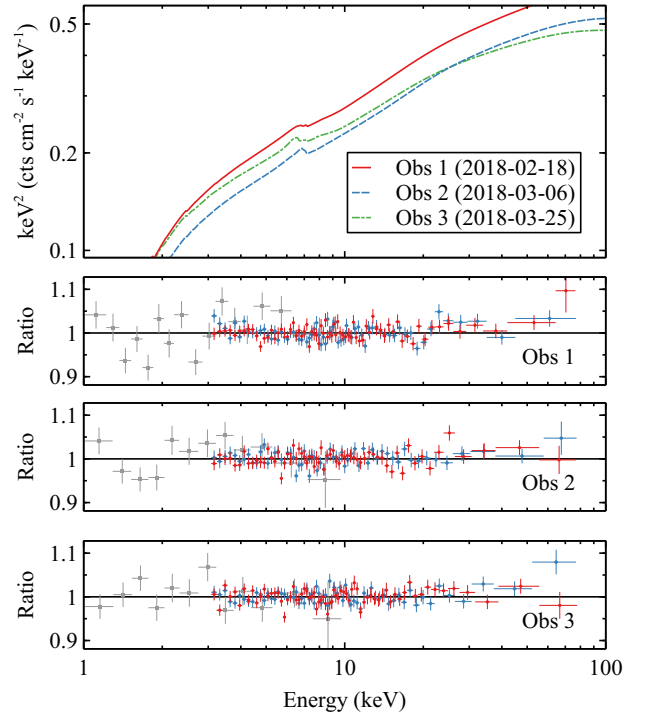


Figure 9. Top: best-fit `relxill1pcp` models for each individual observation. Bottom: corresponding data/model ratio plots for each epoch. $F_{3-78\text{keV}}$ is absorption-corrected X-ray flux in the *NuSTAR* band (3–78 keV).

Table 3. Best-fit parameters for each observation of MAXI J1813. $F_{1-78\text{keV}}$ is the unabsorbed flux of MAXI J1813 in units of $10^{-9} \text{ erg cm}^{-2} \text{ s}^{-1}$. The quoted errors are at the 90% confidence level.

Parameters	Obs1	Obs2	Obs3
$N_{\text{H}} (10^{21} \text{ cm}^{-2})$	8.21 ± 0.02	$8.30^{+0.02}_{-0.03}$	7.92 ± 0.05
$h (r_{\text{g}})$	14^{+9}_{-10}	18^{+6}_{-12}	18^{+22}_{-14}
i (deg)	-	23 ± 10	-
$R_{\text{in}} (r_{\text{g}})$	< 9	< 14	< 13
Γ	$1.620^{+0.015}_{-0.012}$	1.651 ± 0.007	$1.681^{+0.011}_{-0.010}$
kT_{e} (keV)	> 200	> 180	> 150
$Z_{\text{Fe}} (Z_{\odot})$	-	1.5 ± 0.5	-
f_{eff}	0.18 ± 0.03	$0.18^{+0.02}_{-0.04}$	$0.18^{+0.04}_{-0.03}$
$\log(\xi / \text{erg cm s}^{-1})$	$3.18^{+0.10}_{-0.12}$	2.8 ± 0.2	$3.11^{+0.11}_{-0.20}$
Norm (10^{-3})	$6.5^{+0.6}_{-1.4}$	$4.7^{+0.2}_{-0.4}$	$4.3^{+0.6}_{-0.4}$
C_{FPMB}	1.020 ± 0.004	1.017 ± 0.004	$1.027^{+0.003}_{-0.005}$
C_{XRT}	1.031 ± 0.018	$1.031^{+0.017}_{-0.020}$	1.02 ± 0.02
$F_{1-78\text{keV}}$	$2.193^{+0.008}_{-0.010}$	$1.811^{+0.013}_{-0.012}$	1.866 ± 0.013
χ^2/ν		$2907.72/2826$	

mass of $10 M_{\odot}$, MAXI J1813 is accreting at an Eddington ratio of $\lambda_{\text{Edd}} = 1 - 2\%$.

We find that most of the model parameters are consistent among three epochs, e.g. the inner radius of the disc, the height of the corona and the reflection fraction of the reflection component. The main difference of the spectra from the three observations is the photon index of the coronal Comptonisation continuum emission. The third observation has the softest continuum emission of

$\Gamma \approx 1.68$ while the first observation has the hardest continuum emission of $\Gamma \approx 1.62$.

5 DISCUSSION

We analyse the *NuSTAR* and *Swift* spectra of MAXI J1813 in outburst in 2018. During the outburst, MAXI J1813 remains in the canonical hard state. The *NuSTAR* observations of MAXI J1813 show evidence of reflected emission from the inner region of the accretion disc.

By modelling the reflection spectra with a lamppost model, we find a disc inner radius of $R_{\text{in}} < 7 r_g$ and a small inclination angle of around 23° . The abundances are found to be close to solar values. This suggests either a slightly truncated disc or a non-truncated disc forms at a few per cent of the Eddington limit in MAXI J1813. The measurements of these parameters are consistent when a power-law emissivity profile or a high disc density is applied instead.

5.1 The Disc Reflection Spectrum of MAXI J1813

In Section 3.3, we consider a disc reflection model with a variable density parameter, although such a model does not significantly improve the fit. The data show tentative evidence of a high disc density of $n_e \approx 10^{19} \text{ cm}^{-3}$ in MAXI J1813. But only an upper limit of $n_e \approx 10^{21} \text{ cm}^{-3}$ (90% confidence range) is obtained. When a $n_e \approx 10^{19} \text{ cm}^{-3}$ model is considered, the key parameters of the model, e.g. i and R_{in} , are consistent with those achieved by a low-density disc model.

The reflection models for the three epochs are mostly consistent, suggesting the same geometry of the innermost accretion for the period of *NuSTAR* observations. The inner radius of the disc remains a small value with an upper limit of $9\text{--}14 r_g$, and the corona remains within a region of $\approx 10\text{--}20 r_g$. The disc reflection fraction parameter is consistently around 0.18 for all three epochs. Therefore, we conclude that the multi-epoch variability of MAXI J1813 observed by *NuSTAR* is dominated only by the variable photon index of the X-ray continuum emission.

5.2 The Inner Radius of the Disc in MAXI J1813

Recent work on reflection modelling of BH X-ray binaries in the hard state focuses on the measurement of the inner disc radius. Whether the disc is significantly truncated or close to the ISCO at a modest luminosity, e.g. $L_X = 0.01\text{--}0.1 L_{\text{Edd}}$, remains a disputed question.

For example, García et al. (2015) analysed the *RXTE* spectra of GX 339–4 in the hard state. They found that the disc inner radius of this object moves outwards to $4.6 r_g$ when its luminosity decreases from around 17% to 1% of Eddington. At the highest luminosity, the inner radius is consistent with the ISCO for a high BH spin of $a_* \approx 0.95$. Similar results were found in Reis et al. (2008); Wang-Ji et al. (2018); Jiang et al. (2019a) where different models and data were used. In particular, Jiang et al. (2019a) fit the high density disc reflection model to the *NuSTAR* observations of this object in 2013 and 2015. In the 2013 outburst, GX 339–4 failed to transit to the soft state. No significantly different measurements of R_{in} were found in the full outburst and the failed-transition outburst of this object (see Fig. 8 in Jiang et al. 2019a).

In comparison, Plant et al. (2015) found the disc in GX 339–4 is extremely truncated at $300 r_g$ by fitting its *XMM-Newton* observations in the hard state. A similar conclusion was found in

Kolehmainen et al. (2013). The disagreement between two completely different conclusions may be due to the calibration issues of the timing mode data with pile-up effects from *XMM-Newton* (García et al. 2015), which was noted by Kolehmainen et al. (2013).

Similar efforts have been made for other objects too. For instance, GRS 1716–249 has been found to show a small inner radius of $< 20 r_g$ by Jiang et al. (2020a). Tao et al. (2019), however, found a much tighter constraint based on the same observation. They argued that the inner disc is consistent with ISCO for a high BH spin of > 0.92 . Different models were considered in these two pieces of work. The former modelled only the disc reflection spectra in GRS 1716–249. The latter was obtained by fitting both the disc thermal and reflection spectra. Instead of applying a Comptonised disc model to the disc thermal emission (e.g. Steiner et al. 2010), Tao et al. (2019) fit the unscattered disc thermal emission component with a relativistic disc model. Disagreement was found in other objects too, e.g. MAXI J1820+070 (Buisson et al. 2019; Zdziarski et al. 2021a) and XTE J1752–223 (García et al. 2018; Zdziarski et al. 2021b).

We report the first measurements of R_{in} in MAXI J1813 using reflection spectroscopy. The observations were taken during the hard state of this source when $L_X \approx 1\text{--}2\% L_{\text{Edd}}$. We find all three epochs are consistent with an inner disc radius smaller than $9\text{--}15 r_g$. Assuming a maximum BH spin, the disc is either consistent with ISCO or slightly truncated. The choice of BH spin in our model does not affect our measurements of R_{in} (see Appendix B). By stacking the spectra of three epochs, we obtain a tighter constraint of $R_{\text{in}} (< 7 r_g)$. This result is similar to the measurements for some other objects at a similar Eddington ratio (e.g. Wang et al. 2012; Xu et al. 2018; Jiang et al. 2020a).

Lastly, we note that previous analysis for some other sources in the hard state obtained a much tighter constraint on the disc inner radius and a more compact coronal geometry (e.g. Fabian et al. 2012; Parker et al. 2015; Wang-Ji et al. 2018; Xu et al. 2018). Moreover, Xu et al. (2018) found that the broken power-law and lamppost emissivity profiles offer a different measurement for the disc inclination angle of MAXI J1535–571. Differences due to systematic uncertainties in the disc reflection spectroscopy are expected when different flavours of reflection models are used (e.g. see the latest review in Bambi et al. 2021).

However, we can only achieve an upper limit of $R_{\text{in}} < 7 r_g$ for MAXI J1813 (see Table 2). Our model also suggests a slightly extended corona of $h \approx 10\text{--}20 r_g$. Statistical uncertainties dominate over the systematic uncertainties of reflection spectroscopy in our case, because the contribution of the disc reflection component to the total X-ray flux is low in MAXI J1813. For instance, f_{refl} is 1.5 (0.6) when a lamppost (broken power-law) emissivity profile is applied to the hard state observation of MAXI J1535–571. In comparison, $f_{\text{refl}} = 0.19$ (0.08) is found for MAXI J1813 when a lamppost (broken power-law) emissivity profile is used. The low f_{refl} in MAXI J1813 might result from its slightly larger coronal region than the ones in other sources (e.g. $h < 10 r_g$, Fabian et al. 2012; Parker et al. 2015; Xu et al. 2018).

6 CONCLUSIONS

We have performed a detailed analysis of the *NuSTAR* and *Swift* spectra from observations of the hard state of MAXI J1813. During the period of observations, the X-ray luminosity was $1\text{--}2\%$ of Eddington. The observed broad Fe K emission cannot be modelled by narrow reflection features. A relativistic disc reflection model is

thus applied to the data. We find, in agreement with several objects in a similar Eddington ratio (e.g. [García et al. 2015](#)), that the inner radius of the disc is close to the ISCO ($R_{\text{in}} < 7r_g$, 90% confidence uncertainty range). Multi-epoch spectral analysis is also performed. We find that the spectral difference between epochs results from the variable primary continuum emission from the corona while the geometry of the innermost accretion region remains consistent.

ACKNOWLEDGEMENTS

This paper was written during the worldwide COVID-19 pandemic in 2020–2022. We acknowledge the hard work of all the health care workers around the world. We would not be able to finish this paper without their protection. J.J. acknowledges support from the Leverhulme Trust, the Isaac Newton Trust and St Edmund’s College, University of Cambridge.

DATA AVAILABILITY

All the data can be downloaded from the HEASARC website at <https://heasarc.gsfc.nasa.gov>. The `reflionx` and `relxill` models used in this work are available for downloads at <https://www.michaelparker.space/reflionx-models> and <http://www.sternwarte.uni-erlangen.de/dauser/research/relxill>.

REFERENCES

- Armas Padilla M., Muñoz-Darias T., Sánchez-Sierras J., De Marco B., Jiménez-Ibarra F., Casares J., Corral-Santana J. M., Torres M. A. P., 2019, *MNRAS*, **485**, 5235
- Arnaud K. A., 1996, *XSPEC: The First Ten Years*
- Bambi C., et al., 2021, *Space Sci. Rev.*, **217**, 65
- Basak R., Zdziarski A. A., Parker M., Islam N., 2017, *MNRAS*, **472**, 4220
- Blandford R. D., Znajek R. L., 1977, *MNRAS*, **179**, 433
- Brocksopp C., Bandyopadhyay R. M., Fender R. P., 2004, *New Astron.*, **9**, 249
- Buisson D. J. K., et al., 2019, *MNRAS*, **490**, 1350
- Chruściel P. T., Costa J. L., Heusler M., 2012, *Living Reviews in Relativity*, **15**, 7
- Connors R. M. T., et al., 2021, *ApJ*, **909**, 146
- Cui W., Ebisawa K., Dotani T., Kubota A., 1998, *ApJ*, **493**, L75
- Dauser T., García J., Wilms J., Böck M., Brenneman L. W., Falanga M., Fukumura K., Reynolds C. S., 2013, *MNRAS*, **430**, 1694
- Dauser T., García J., Walton D. J., Eikmann W., Kallman T., McClintock J., Wilms J., 2016, *A&A*, **590**, A76
- De Marco B., Ponti G., Cappi M., Dadina M., Uttley P., Cackett E. M., Fabian A. C., Miniutti G., 2013, *MNRAS*, **431**, 2441
- Done C., Gierliński M., Kubota A., 2007, *A&ARv*, **15**, 1
- Dunn R. J. H., Fender R. P., Körding E. G., Belloni T., Cabanac C., 2010, *MNRAS*, **403**, 61
- Esin A. A., McClintock J. E., Narayan R., 1997, *ApJ*, **489**, 865
- Fabian A. C., Rees M. J., Stella L., White N. E., 1989, *MNRAS*, **238**, 729
- Fabian A. C., et al., 2012, *MNRAS*, **424**, 217
- Fender R. P., Belloni T. M., Gallo E., 2004, *MNRAS*, **355**, 1105
- Foreman-Mackey D., Hogg D. W., Lang D., Goodman J., 2013, *PASP*, **125**, 306
- Fuerst F., et al., 2018, *The Astronomer’s Telegram*, **11357**, 1
- Fürst F., et al., 2015, *ApJ*, **808**, 122
- García J., Kallman T. R., 2010, *ApJ*, **718**, 695
- García J. A., Steiner J. F., McClintock J. E., Remillard R. A., Grinberg V., Dauser T., 2015, *ApJ*, **813**, 84
- García J. A., Fabian A. C., Kallman T. R., Dauser T., Parker M. L., McClintock J. E., Steiner J. F., Wilms J., 2016, *MNRAS*, **462**, 751
- García J. A., et al., 2018, *ApJ*, **864**, 25
- Gonzalez A. G., Wilkins D. R., Gallo L. C., 2017, *MNRAS*, **472**, 1932
- Goodman J., Weare J., 2010, *Communications in Applied Mathematics and Computational Science*, Vol.~5, No.~1, p.~65-80, 2010, **5**, 65
- Hertz P., Grindlay J. E., 1983, *ApJ*, **275**, 105
- Homan J., Miller J. M., Wijnands R., van der Klis M., Belloni T., Steeghs D., Lewin W. H. G., 2005, *ApJ*, **623**, 383
- Jana A., et al., 2021, arXiv e-prints, p. arXiv:2104.12924
- Jiang J., et al., 2018, *MNRAS*, **477**, 3711
- Jiang J., Fabian A. C., Wang J., Walton D. J., García J. A., Parker M. L., Steiner J. F., Tomsick J. A., 2019a, *MNRAS*, **484**, 1972
- Jiang J., et al., 2019b, *MNRAS*, **489**, 3436
- Jiang J., Fürst F., Walton D. J., Parker M. L., Fabian A. C., 2020a, *MNRAS*, **492**, 1947
- Jiang J., Gallo L. C., Fabian A. C., Parker M. L., Reynolds C. S., 2020b, *MNRAS*, **498**, 3888
- Jordán A., et al., 2004, *ApJ*, **613**, 279
- Jurić M., et al., 2008, *ApJ*, **673**, 864
- Kara E., et al., 2019, *Nature*, **565**, 198
- Kawase T., et al., 2018, *The Astronomer’s Telegram*, **11323**, 1
- Kolehmainen M., Done C., Díaz Trigo M., 2013, *Monthly Notices of the Royal Astronomical Society*, **437**, 316
- Liu Q. Z., van Paradijs J., van den Heuvel E. P. J., 2006, *A&A*, **455**, 1165
- Liu Q. Z., van Paradijs J., van den Heuvel E. P. J., 2007, *A&A*, **469**, 807
- Madsen K. K., et al., 2015, *ApJS*, **220**, 8
- Martocchia A., Matt G., 1996, *MNRAS*, **282**, L53
- Matsuoka M., et al., 2009, *PASJ*, **61**, 999
- McClintock J. E., Narayan R., Steiner J. F., 2014, *Space Sci. Rev.*, **183**, 295
- Oda M., Gorenstein P., Gursky H., Kellogg E., Schreier E., Tananbaum H., Giacconi R., 1971, *ApJ*, **166**, L1
- Parker M. L., et al., 2015, *ApJ*, **808**, 9
- Plant D. S., Fender, R. P. Ponti, G. Muñoz-Darias, T. Coriat, M. 2015, *A&A*, **573**, A120
- Quataert E., Narayan R., 1999, *The Astrophysical Journal*, **520**, 298
- Rao A. R., Yadav J. S., Paul B., 2000, *ApJ*, **544**, 443
- Reis R. C., Fabian A. C., Ross R. R., Miniutti G., Miller J. M., Reynolds C., 2008, *MNRAS*, **387**, 1489
- Reis R. C., Miller J. M., Reynolds M. T., Fabian A. C., Walton D. J., Cackett E., Steiner J. F., 2013, *ApJ*, **763**, 48
- Ross R. R., Fabian A. C., 2007, *MNRAS*, **381**, 1697
- Russell T. D., Miller-Jones J. C. A., Sivakoff G. R., Tetarenko A. J., JACPO T XRB Collaboration 2018, *The Astronomer’s Telegram*, **11356**, 1
- Shidatsu M., et al., 2011, *PASJ*, **63**, S803
- Steiner J. F., McClintock J. E., Remillard R. A., Gou L., Yamada S., Narayan R., 2010, *ApJ*, **718**, L117
- Sturmer S. J., Shrader C. R., 2005, *ApJ*, **625**, 923
- Tao L., Tomsick J. A., Qu J., Zhang S., Zhang S., Bu Q., 2019, *ApJ*, **887**, 184
- Tchekhovskoy A., Narayan R., McKinney J. C., 2011, *MNRAS*, **418**, L79
- Tomsick J. A., et al., 2018, *ApJ*, **855**, 3
- Wang-Ji J., et al., 2018, *ApJ*, **855**, 61
- Wang H., Zhou H., Yuan W., Wang T., 2012, *ApJ*, **751**, L23
- Wilkins D. R., Fabian A. C., 2012, *MNRAS*, **424**, 1284
- Willingale R., Starling R. L. C., Beardmore A. P., Tanvir N. R., O’Brien P. T., 2013, *MNRAS*, **431**, 394
- Wilms J., Nowak M. A., Pottschmidt K., Pooley G. G., Fritz S., 2006, *A&A*, **447**, 245
- Xu Y., et al., 2018, *ApJ*, **852**, L34
- Yu W., Yan Z., 2009, *ApJ*, **701**, 1940
- Zdziarski A. A., You B., Szanecki M., Li X.-B., Ge M.-Y., 2021a, arXiv e-prints, p. arXiv:2112.08116
- Zdziarski A. A., De Marco B., Szanecki M., Niedźwiecki A., Markowitz A., 2021b, *ApJ*, **906**, 69
- Zhang S. N., Cui W., Chen W., 1997, *ApJ*, **482**, L155
- Życki P. T., Done C., Smith D. A., 1999, *MNRAS*, **309**, 561

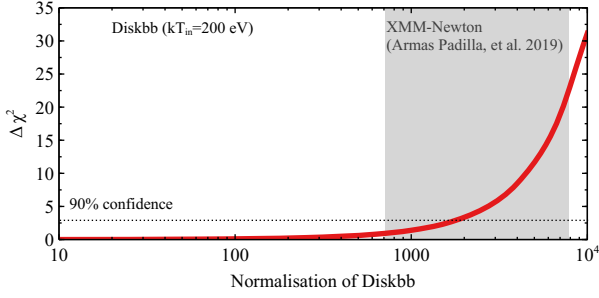


Figure A1. χ^2 distribution against the normalisation parameter of the `diskbb` model for the stacked spectra of MAXI J1813. The temperature is fixed at 200 eV, the best-fit value for the *XMM-Newton* observations of MAXI J1813 (Armas Padilla et al. 2019). Only an upper limit of 2000 is obtained for this component, corresponding to 1.8% of the total X-ray luminosity. The grey shaded region shows the uncertainty range of the normalisation parameter given by the *XMM-Newton* observations of the same source.

APPENDIX A: THERMAL EMISSION IN THE HARD STATE OF MAXI J1813

Archival *XMM-Newton* timing-mode observations of MAXI J1813 at the beginning of the outburst show some evidence of weak thermal emission in the soft X-ray band. This thermal component is consistent with disk blackbody emission of $kT_{\text{in}} \approx 200$ eV (Armas Padilla et al. 2019). However, the contribution of this component to the total X-ray luminosity is low, e.g. $<2\%$ (Armas Padilla et al. 2019).

We estimate the upper limit of such a thermal component in our data by adding an additional `diskbb` model. The kT_{in} parameter is fixed at 200 eV, the value inferred from *XMM-Newton* observations (Armas Padilla et al. 2019). We show the χ^2 distribution against the normalisation parameter of `diskbb`. Only an upper limit of 2000 (90% confidence) is obtained. At this upper limit, the `diskbb` component takes up only 1.8% of the total luminosity in the 0.01–1000 keV band. We, therefore, conclude that there is no significant evidence of thermal emission in our observations.

APPENDIX B: THE INNER RADIUS OF THE DISC AND BH SPIN

The BH spin parameter a_* is fixed at 0.998 in Section 3 to investigate the possibility of R_{in} in the range of small values. In this appendix, we study whether the choice of a_* affects our measurements of R_{in} .

We consider the same reflection model `relxill1pcp` as in Section 3. a_* is fixed at 0.5, the corresponding R_{ISCO} of which is $4.32 r_g$. The lower limit of R_{in} is thus at $4.32 r_g$. We obtain a similarly good fit to the spectra of MAXI J1813 with $\chi^2/\nu = 1168.40/1106$. χ^2 is slightly higher than the value in Section 3 where $a_* = 0.998$. Best-fit parameters are shown in Table B1 and best-fit model is shown in Fig. B1.

The $a_* = 0.5$ and $a_* = 0.998$ models provide consistent measurements of all the parameters. In particular, we show χ^2 distribution of R_{in} in Fig. B2. The 90% confidence uncertainty ranges of R_{in} by two models are consistent. The difference is that the $a_* = 0.998$ model allows R_{in} to be lower than $4.32 r_g$. In conclusion, the measurement of R_{in} is unaffected by our choice of $a_* = 0.998$ in Section 3.

Table B1. Best-fit parameters for the stacked spectra of MAXI J1813. In this fit, the BH spin parameter is fixed at 0.5. The corresponding radius of the ISCO is $0.43 r_g$.

Parameters	Values
N_{H} (10^{21} cm^{-2})	$8.10^{+0.02}_{-0.03}$
h (r_g)	12^{+7}_{-5}
i (deg)	23^{+12}_{-10}
R_{in} (r_g)	<7
Γ	1.645 ± 0.006
kT_e (keV)	>180
Z_{Fe} (Z_{\odot})	$1.6^{+0.4}_{-0.5}$
f_{refl}	$0.19^{+0.04}_{-0.03}$
$\log(\xi/\text{erg cm s}^{-2})$	3.09 ± 0.07
Norm (10^{-3})	5.8 ± 0.2
C_{FPMB}	1.025 ± 0.003
C_{XRT}	1.03 ± 0.03
χ^2/ν	$1168.40/1106$

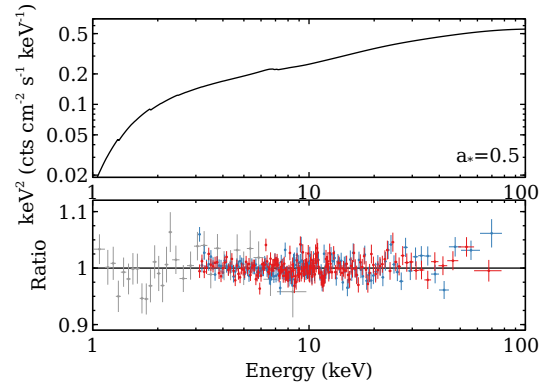


Figure B1. Top: best-fit `relxill1pcp` model. Bottom: corresponding data/model ratio (red: FPMA; blue: FPMB; grey: XRT). In this model, we fix a_* at 0.5. The `relxill1pcp` model with $a_* = 0.998$ is used in Fig. 5. Two models provide a similar fit to the spectra of MAXI J1813.

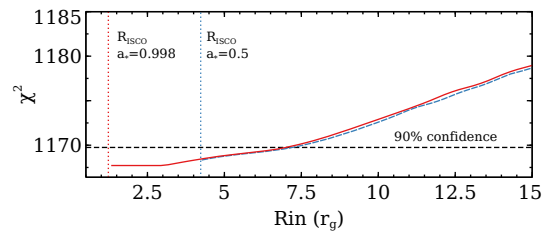


Figure B2. χ^2 as a function of R_{in} with different assumptions of a_* in the reflection model (red solid line: $a_* = 0.998$; blue dashed line: $a_* = 0.5$). Two models provide similar constraints on R_{in} . The red and blue vertical dotted lines show the radius of the ISCO for $a_* = 0.998$ ($R_{\text{ISCO}} = 1.23 r_g$) and $a_* = 0.5$ ($R_{\text{ISCO}} = 4.23 r_g$).

This paper has been typeset from a \LaTeX file prepared by the author.